THE JOURNAL OF PHYSICAL CHEMISTRY C
A JOURNAL OF THE AMERICAN CHEMICAL SOCIETY

pubs.acs.org/JPCC

Article

Ionic Conduction in Sr-Doped CeF_3 as Studied by ^{19}F NMR and AC Impedance Measurement

Miwa Murakami,* Seiya Matsumoto, and Atsushi Mineshige

Cite This: *J. Phys. Chem. C* 2022, 126, 20135−20142

Read Online

ACCESS | Metrics & More | Article Recommendations

ABSTRACT: Among the three inequivalent fluorides in tysonite CeF_3 (F1, F2, and F3 in the ratio of 12:4:2 per unit cell), we show by ^{19}F solid-state NMR that F1 is solely responsible for the ion conductivity in $Ce_{1-x}Sr_xF_{3-x}$ (x = 0.001) at 0 °C. It is further shown that the observed conductivity can be explained quantitatively by using the Nernst−Einstein relation with the F1−F1 exchange rate (ca. 6×10^5 s^{-1}) estimated from lineshape analysis with the carrier−F1 concentration. As for an alternative method to obtain the hopping rate of a carrier, we adopt the AC impedance method, for which the identity of the "carrier" is rather elusive. The observed AC impedance gives the carrier hopping rate of 3.5×10^7 s^{-1}, which is ca. 60 times of the F1−F1 exchange rate determined by NMR. The slower F1−F1 hopping rate is ascribed to the result of the long-time average of the faster carrier hopping rate. For the AC impedance analysis, the concentration of the carrier to realize the observed conductivity is much larger than that of the fluoride ion vacancy introduced by Sr doping. For explanation, we postulate that what influences AC impedance includes not only the vacancy but also fast-exchanging fluoride ions around the vacancy.

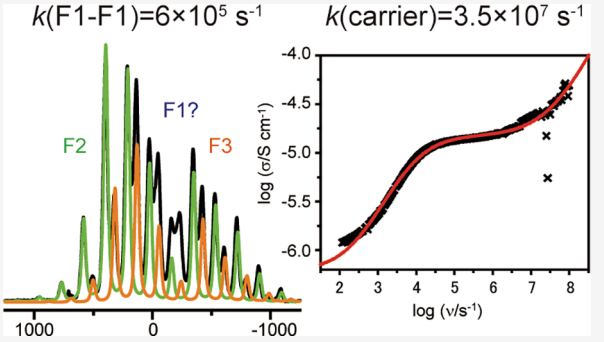

1. INTRODUCTION

Trifluoride with a tysonite structure[1−5] such as LaF_3 and CeF_3 is known to exhibit high ionic conductivity of ca. 10^{-4} S/cm at around room temperature with an introduction of a few percentage of bivalent cation,[6−12] such as Sr^{2+}. Long-standing controversies on ionic conduction pathways among the three crystallographically inequivalent sites in tysonite (F1, F2, and F3 in the ratio of 12:4:2 per unit cell) have recently been settled down by using ^{19}F magic angle spinning (MAS) NMR for LaF_3[13] and CeF_3;[14] F1−F1 exchange occurs first, followed by F1−F3, and F1−F2 exchange is most restricted. So far, a number of solid-state ^{19}F NMR works examined the diffusion of the fluoride ion in tysonite, some of which will be briefly touched upon in the following to compare with the results obtained from the analysis of conductivity.

Schoonman et al.[15] examined the AC impedance of Ba-doped LaF_3. From the conductivity isotherm, they obtained the diffusion coefficient of fluoride ion vacancies (D_v) in LaF_3 at 250 K ($D_v = 3.7 \times 10^{-17}$ m^2/s), which is consistent with the diffusion coefficient of a fluoride ion (D_{nmr}) calculated from the activation parameters obtained by analyzing ^{19}F NMR line-narrowing of LaF_3[16] ($D_{nmr} = 9.2 \times 10^{-17}$ m^2/s). Unfortunately, no details, such as the mean hopping distance for the vacancy as well as its frequency or carrier density, which may be required to deduce D_v, were presented.

Roos et al. reported for nominally pure LaF_3 at 300 K that the diffusion constant obtained by analyzing the temperature dependence of conductivity (D_σ) is equal to that obtained from ^{19}F NMR $T_{1\rho}$ and T_2 measurements ($D_{nmr} \sim D_\sigma \sim 2.6 \times 10^{-17}$ m^2/s).[17,18] They further pointed out that the value is consistent with D_{nmr} obtained by Lee and Sher[16] ($D_{nmr} \sim 2.5 \times 10^{-17}$ m^2/s) for a single crystal of LaF_3. It should be noted, however, in deducing D_{nmr}, that Roos et al. adopted 0.415 nm for the mean hopping distance of the fluoride ion according to their assignment of the fast-moving ion being F2, while Lee and Sher adopted 0.26 nm, which is the average near-neighbor F−F distance in LaF_3. Hence, the apparent agreement between the two D_{nmr} values is questionable.

Breuer et al. obtained $D_{nmr} = 1.9 \times 10^{-14}$ m^2/s for $La_{0.9}Ba_{0.1}F_{2.9}$ at 373 K from the jump rate (1.3×10^6 s^{-1}) of F^- ion determined by ^{19}F $T_{1\rho}$ measurement and the average jump distance of 0.3 nm.[19] The authors indicated that this value agrees very well with $D_\sigma = 0.8 \times 10^{-14}$ m^2/s calculated from conductivity. Unfortunately, however, the authors did not give the DC conductivity (σ_{dc}) at 373 K nor the concentration of charge carriers to follow their estimation of D_σ.

Received: August 30, 2022
Revised: October 27, 2022
Published: November 18, 2022

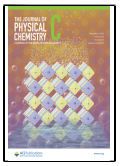

https://doi.org/10.1021/acs.jpcc.2c06215
J. Phys. Chem. C 2022, 126, 20135−20142

Sorokin and Sobolev[10] presented a detailed procedure for analysis of frequency dependence of conductivity (AC impedance) and applied to various doped tysonite single crystals. They adopted an empirical universal response equation for frequency response of conductivity ($\sigma(\nu)$) postulated by Almond and co-workers[20−22] (hereafter, the AC impedance method), which may be written as

$$\sigma(\nu) = \sigma_{dc}\{1 + (\nu/\nu_c)^{\alpha}\} \quad (1)$$

where ν is the modulation frequency of the electric field and α is a constant ($0 < \alpha < 1$). Almond and co-workers interpreted the characteristic frequency ν_c as the thermally activated carrier hopping rate (k_v, hereafter). Sorokin and Sobolev assumed that the carrier is the ion vacancy and calculated its mobility by using the Nernst−Einstein relation

$$\mu = Ze_0k_v\ a^2/6k_BT \quad (2)$$

where Z is valence of carrier ($Z = 1$ for the present case), e_0 is the elementary charge, k_B is the Boltzmann constant, and a is the mean hopping distance of the vacancy. The mobility of the ion vacancy is related to σ_{dc} as

$$\sigma_{dc} = e_0C_v\mu \quad (3)$$

where C_v is the concentration of the vacancy. They further assumed that the vacancy is solely brought about by doping. Hence C_v for $La_{1-x}Sr_xF_{3-x}$ is given by

$$C_v = 6x/V \quad (4)$$

where V is the unit cell volume of tysonite. Then, the hopping distance a was used as an adjustable parameter to realize the observed DC conductivity. For example, $a = 0.55$ nm was obtained for $La_{1-x}Sr_xF_{3-x}$ ($x = 0.05$) at 254.6 K. This value is much longer than $a \sim 0.26$ nm adopted by Lee and Sher,[16] and for explanation of this long distance, the authors postulated F1−F1 exchange between two F1 layers via vacancy at the F2 atom. This is rather confusing as such exchange would lead the F1−F2 distance to be the hopping distance for the vacancy. Furthermore, it is widely accepted that the vacancy is at the F1 site.[12,23−25] If one adopts $a \sim 0.26$ nm and use the carrier density C_v as an adjustable parameter, C_v becomes ca. 4.5 times larger than the value given by eq 4.

The AC impedance method is useful as it gives the carrier hopping rate, which can be compared directly with a motional rate obtained by an NMR experiment. However, it should be pointed out that the identity of the characteristic frequency ν_c as the hopping rate has been questioned.[26] Furthermore, comparison of the results of NMR and the AC impedance method is not straightforward, as while ^{19}F NMR directly observes the fluoride ion, AC impedance is governed by the so-called "carrier", whose identity is rather elusive. Moreover, the characteristic timescale of observation is different not only between NMR and the AC impedance method but also among NMR measurements, such as relaxation (T_1, $T_{1\rho}$, and T_2) and lineshape measurements. With these reservations in mind, we adopt the AC impedance method in this work to compare ν_c with the rate obtained by NMR.

First, we examine temperature dependence of conductivity and obtain the carrier hopping rate k_v in $Ce_{1-x}Sr_xF_{3-x}$ ($x = 0.001$) at 0 °C by the AC impedance method. The diffusion coefficient D_v is evaluated with the mean hopping distance a being the average F1−F1 nearest-neighbor distance of 0.26 nm. Then, the conductivity σ is elucidated by using eqs 2 and 3, with the carrier density C_v as an adjustable parameter. Furthermore, we examine C_v for the $Ce_{1-x}Sr_xF_{3-x}$ ($x = 0$, 0.005, and 0.01) samples similarly to examine x dependence of C_v and the identity of the "carrier" viewed from the AC impedance is discussed.

Second, we extend our ^{19}F-NMR study[14] of Sr-doped CeF_3 to estimate motional frequency of fluoride ions. We show for $Ce_{1-x}Sr_xF_{3-x}$ ($x = 0.001$) at around room temperature that, while the F2 and F3 lineshapes are almost identical to those of nondoped "pristine" CeF_3, the apparent F1 signal intensity is different from that in pristine CeF_3, and its intensity decreases appreciably. The F1−F1 exchanging rate k_F in $Ce_{1-x}Sr_xF_{3-x}$ ($x = 0.001$) at 0 °C is estimated from the observed reduction of the F1 signal, and the diffusion coefficient is evaluated with the hopping distance a of 0.26 nm. We show that the conductivity σ is consistent with the calculated one using eqs 2 and 3, considering F1 is the carrier. In other words, ion conduction in $Ce_{1-x}Sr_xF_{3-x}$ ($x = 0.001$) at 0 °C is solely governed by the F1 exchange motion from the point of view of ^{19}F NMR.

Lastly, the apparent difference in the carrier hopping rate k_v obtained by the AC impedance method and the F1 hopping rate k_F obtained from ^{19}F NMR lineshape is discussed on the basis of the characteristic timescale of each observation.

2. EXPERIMENTAL METHODS

2.1. Sample Preparation. CeF_3 and SrF_2 were purchased from Kojundo Chemical Laboratory Co. Ltd. (99.9%) and used without further purification. We refer to the as-it-is CeF_3 sample as pristine CeF_3. The $Ce_{1-x}Sr_xF_{3-x}$ samples ($x = 0$, 0.001, 0.005, and 0.01) were prepared from a mixture of CeF_3 and SrF_2 powders in different ratios. The mixture was ball milled at room temperature with the rotation speed of 300 rpm for 3 h. The powders were then uniaxially pressed into pellet at 87 MPa, whose diameter is 12 mm, and additionally pressed by cold isostatic pressing at 200 MPa. Furthermore, the pellets were fired at 1000 °C for 1 h in a dry Ar atmosphere. The powder X-ray diffraction (XRD) patterns for the $x = 0.001$ and 0.01 samples were shown in ref 14. The XRD patterns for the other samples are consistent with those for $x = 0.001$ and 0.01. The pellet for pristine CeF_3 for conductivity measurement was prepared similarly from the as-it-is CeF_3 sample without milling−firing. Each of the pellet $Ce_{1-x}Sr_xF_{3-x}$ samples ($x = 0$, 0.001, 0.005, and 0.01) was ground in an agate mortar to a powder for NMR measurement.

2.2. Impedance Measurement. AC impedance measurements were conducted using an impedance analyzer (E4990A, Keysight Technologies). Both faces of the disk-shaped, fired $Ce_{1-x}Sr_xF_{3-x}$ samples (diameter of ∼12 mm and thickness of ∼1 mm) were coated with platinum as electrodes using a magnetron sputtering apparatus (MSP-20TK vacuum device). These samples were loaded into a cell to measure the AC impedance under controlled atmospheres at temperatures between 233 and 353 K (ZF-ST-HG, Qualtec Co. Ltd.). The applied voltage was fixed at 20 mV, and measurements were taken within a frequency range of 100 Hz to 100 MHz in a high-purity Ar. The electrical conductivity evaluated from the AC impedance could be equated with the ionic conductivity of the F ions, because it is expected that the ionic transport number of $Ce_{1-x}Sr_xF_{3-x}$ is approximately 1.

2.3. NMR Analysis. The NMR measurements were made using the OPENCORE spectrometer[27] operating at 4.7 T with a MAS probe (Agilent Technologies, Inc.) for a 1.6 mm rotor. The resonance frequency for ^{19}F was 188.4 MHz. The ^{19}F MAS spectra were observed by using the Hahn echo sequence

https://doi.org/10.1021/acs.jpcc.2c06215
J. Phys. Chem. C 2022, 126, 20135−20142

under the MAS spinning frequency of 35 kHz with the $\pi/2$ and π pulse lengths being 1.15 and 2.25 μs, respectively. The pulse repetition time was 50 ms. The ^{19}F chemical shifts were calibrated in ppm relative to CCl_3F adopting the ^{19}F chemical shift for neat C_6F_6 (−163 ppm[28]) as an external reference. The temperature calibration experiment was done using ^{207}Pb NMR of $Pb(NO_3)_2$.[29]

3. RESULTS AND DISCUSSION

3.1. AC Impedance Measurements. Figure 1 shows impedance Nyquist plot of $Ce_{1-x}Sr_xF_{3-x}$ (x = 0.001) measured

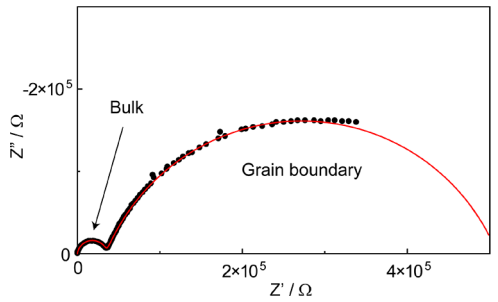

Figure 1. Impedance Nyquist plot of $Ce_{1-x}Sr_xF_{3-x}$ (x = 0.001) measured at 0 °C. The red line through the observed data (the filled balls) is the fitted one.

at 0 °C. The choice of this particular sample and the temperature will be explained in Section 3.2. In Figure 1, two arcs owing to the bulk and grain boundary resistances were clearly observed. By using a curve-fitting procedure, each resistance could be evaluated separately, even if both have similar time constants. Figure 2 shows the temperature

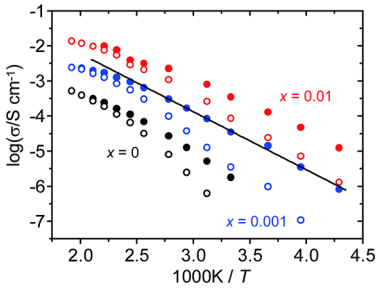

Figure 2. Temperature dependence of the total (open circle) and the bulk (filled circle) conductivities for $Ce_{1-x}Sr_xF_{3-x}$; black (x = 0), blue (x = 0.001), and red (x = 0.01). The straight line through the blue filled balls is for eye-guidance.

dependence of the total electrical conductivity and that for the inner grain of the CeF_3 crystalline bulk regions (the bulk conductivity, σ_{bulk}). For clarity, the results for $Ce_{1-x}Sr_xF_{3-x}$ (x = 0.005) and pristine CeF_3 were not included. For pristine CeF_3, we could not separate bulk and grain boundary resistances due to large contribution of grain boundaries, and the observed total conductivity is lower than that of $Ce_{1-x}Sr_xF_{3-x}$ (x = 0) by ca. 3 orders of magnitude for the temperature range we studied. Even considering the reduction of the apparent conductivity of pristine CeF_3 by grain boundary resistance, the inner grain conductivity of pristine CeF_3 is expected to be much lower than that of $Ce_{1-x}Sr_xF_{3-x}$ (x = 0). The enhancement of the conductivity for Sr-nondoped $Ce_{1-x}Sr_xF_{3-x}$ (x = 0) should be attributed to the milling process, followed by the firing at 1000 °C for 3 h. It is thus envisaged that the milling−firing process introduces defects to facilitate F1 motion, which will be examined quantitatively afterward.

The σ_{bulk} value for $Ce_{1-x}Sr_xF_{3-x}$ (x = 0) at 500 K is ca. 4 × 10^{-4} S/cm, which is comparable to the values of ca. 1 × 10^{-3} S/cm reported previously.[7,8,10,11] From the Arrhenius-type plot for $\log(\sigma_{bulk}T) \propto -E_a/kT$ (not shown), we have an activation energy of ca. 0.4 eV for $Ce_{1-x}Sr_xF_{3-x}$ (x = 0), which is also consistent with the reported values.[7,8,10,12] As is well known, Sr doping improves the conductivity, and the σ_{bulk} value for $Ce_{1-x}Sr_xF_{3-x}$ (x = 0.01) at 300 K becomes 3 × 10^{-4} S/cm, which is also comparable to those reported for Sr-doped CeF_3.[9,11,12]

The apparent reduction of the high-temperature slope in Figure 2 has also been reported for CeF_3[6,7] and LaF_3.[6,15,18,30,31] Omari et al. suggested that, at the slope change temperature, the F2/F3 ions starts to be involved in ion exchange.[32] The onset of F2 and F3 motion in LaF_3 is, for example, suggested from the observed increase of the relative intensity ratio of the ^{19}F NMR signals, F1/F2 + F3, from 2.0 at 450 K to 2.3 at 490 K.[33] Goldman and Shen also reported that ion exchange between inequivalent sites (F1 and F2 + F3) occurs at 415 K in LaF_3.[34] For $Ce_{1-x}Sr_xF_{3-x}$ (x = 0.001), F2 motion becomes appreciable as apparent reduction of the ^{19}F NMR signal intensity of F2 at above 393 K (120 °C).[14] Indeed, the deviation of $\sigma(T)$ from the linear dependence as designated by the eye-guiding straight line at the lower temperature region in Figure 2 occurs at around 393 K for $Ce_{1-x}Sr_xF_{3-x}$ (x = 0.001).

Figure 3 shows a projection of the unit cell of CeF_3, in which F1 connections among the first nearest neighbor with the F1−

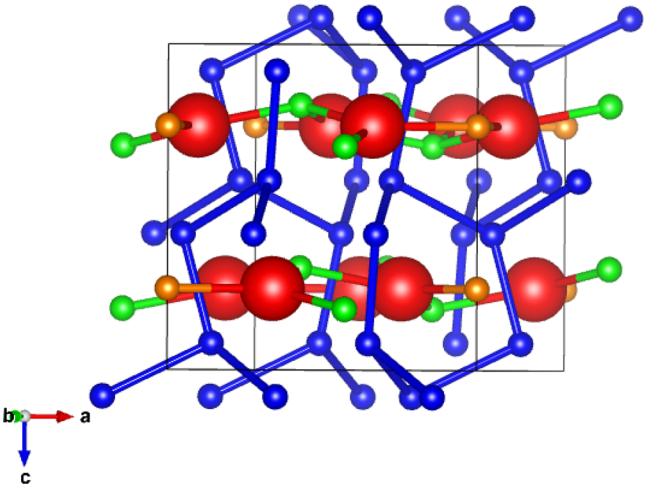

Figure 3. Schematic illustration of F1−F1 connectivity in a unit cell of CeF_3. Red balls are Ce and the three F ions (F1 ∼ F3) are designated by blue, green, and orange, respectively. For simplicity, except for F1−F1 connection (blue sticks), only Ce-F2 and Ce-F3 bonds are drawn.

F1 distance (0.253 nm) and the second neighbors (0.272 nm) are drawn together with the Ce−F2 and Ce−F3 bonds. The F1 network along the c-axis shown in Figure 3 is consistent with the observed anisotropic conductivity in LaF_3;[15] below 415 K, the conductivity in the direction parallel to the c-axis is slightly better than that in the perpendicular direction. The loss of the anisotropy in conduction above 415 K associating with the change of the slope in $\sigma(T)$ is thus attributable to the participation of F2 and F3 ions into ion conduction. A one-

https://doi.org/10.1021/acs.jpcc.2c06215
J. Phys. Chem. C 2022, 126, 20135−20142

dimensional diffusion path along the *c*-axis has also been postulated by analysis of probability density functions.[35]

We show in Figure 4 that, for the concentration range of the dopant Sr^{2+} we studied, ionic conductivity increases almost

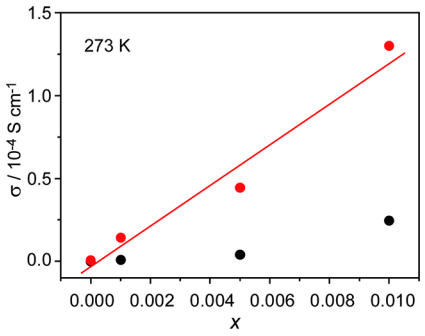

Figure 4. Sr doping ratio (x) dependence of the total (black) and the bulk (red) conductivities for $Ce_{1-x}Sr_xF_{3-x}$ at 0 °C. The straight line through the red balls is for eyeguidance.

linearly with x at 0 °C. The linear dependence is envisaged from the following relation deduced by using eqs 2 and 3 for ion conduction with assuming vacancies introduced by Sr doping acting as the carrier,

$$\sigma = \frac{e_0^2\, C_v\, D_v}{k_B\, T} \tag{5}$$

with the diffusion constant given by

$$D_v = a^2 k_v/6 \tag{6}$$

Here, we assume that the x dependence of C_v is simply written by using eq 4 as

$$C_v(x) = C_v^{\,0} + 6x/V \tag{7}$$

where $C_v^{\,0}$ is the vacancy concentration brought about by the milling−firing procedure in the sample preparation.

Here, we analyze the AC impedance data to elucidate the carrier hopping rate k_v and estimate the diffusion constant for the carrier D_v. Note that we first follow Sorokin and Sobolev[10] to assume naively that the carrier is the ion vacancy. Figure 5 shows the observed frequency dependence of conductivity ($\sigma(\nu)$) of $Ce_{1-x}Sr_xF_{3-x}$ (x = 0.001) at 0 °C. The data consists of two processes with longer and shorter relaxation times, the longer one corresponding to grain boundary response and the shorter one corresponding to ion dynamics in the crystalline

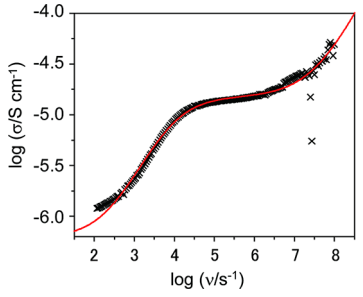

Figure 5. Frequency dependence of conductivity of $Ce_{1-x}Sr_xF_{3-x}$ (x = 0.001) at 0 °C (×). The red curve through the observed data is the least squares one described in the text. The two crosses at log $\nu \sim 7.4$ deviated appreciably from the fitting line are instrumental noises.

bulk regions (the bulk conductivity). For each process, we applied the Almond−West equation (eq 1) as

$$\sigma_i(\nu) = \sigma^0{}_i\{1 + (\nu/k_i)\alpha_i\},\ (i = 1 \text{ or } 2) \tag{8}$$

and the observed $\sigma(\nu)$ values were least squares fitted to $\sigma(\nu) = \sigma_1(\nu)\sigma_2(\nu)/(\sigma_1(\nu) + \sigma_2(\nu))$ by taking $\sigma^0{}_i$, k_i, and α_i (i = 1 or 2) as the adjustable parameters, and the best-fit line is plotted in Figure 5. The best-fit values for the bulk conductivity $\sigma_1^{\,0}$, k_1, and α_1 were $(1.50 \pm 0.07) \times 10^{-5}$ S/cm, $(3.5 \pm 0.5) \times 10^7$ s^{-1}, and 0.79 ± 0.06, respectively. The best-fit $\sigma_1^{\,0}$ value is consistent with the bulk conductivity ($\sigma_{bulk} = 1.43 \times 10^{-5}$ S/cm) obtained by the analysis of the Nyquist plot given in Figure 1.

It is worthy to point out here that the k_1 value (3.5×10^7 s^{-1}) is comparable to the rate (0.9×10^7 s^{-1}) obtained by the AC impedance method for $La_{0.95}Sr_{0.05}F_{2.95}$ at 254.6 K,[10] for which DC conductivity ($\sigma_{dc} = 3.1 \times 10^{-5}$ S/cm) is similar. This consistency is ascribable to their similar structures as well as to the same ionic conduction mechanism.

The diffusion constant of a vacancy estimated by using eq 6 with a = 0.26 nm becomes $D_v = 4.0 \times 10^{-13}$ m^2/s. The concentration of the vacancy C_v in eq 5 is used as an adjustable parameter to realize $\sigma_1^{\,0} = 1.5 \times 10^{-5}$ S/cm, and we have $C_v = 5.6 \times 10^{26}$ m^{-3}, which corresponds to ca. 0.2 vacancies per a unit cell.

We applied the fitting using eq 8 to the AC impedance data of $Ce_{1-x}Sr_xF_{3-x}$ (x = 0, 0.005, and 0.01) at 0 °C and obtained the estimated hopping rate of 4.7×10^6 s^{-1}, 9.7×10^7 s^{-1}, and 9.1×10^7 s^{-1}, respectively. The concentration of the vacancy was estimated similarly for these samples and is plotted together with that obtained for x = 0.001 in Figure 6. The

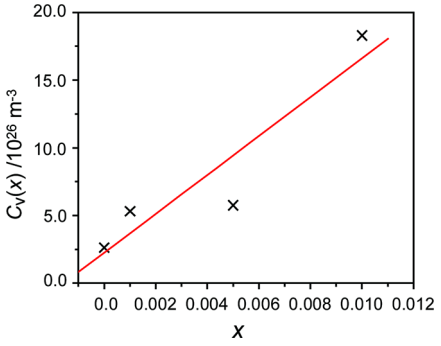

Figure 6. Sr doping ratio (x) dependence of the estimated carrier (vacancy) density in $Ce_{1-x}Sr_xF_{3-x}$. The straight line through the data points is the least squares fitted one described in the text.

straight line in Figure 6 is the result of least squares fitting to eq 7 with the best-fit slope of $(1.4 \pm 0.4) \times 10^{29}$ m^{-3} and the intercept of $C_v^{\,0} = (2.3 \pm 2.2) \times 10^{26}$ m^{-3}. The observed slope is ca. 7 times of that calculated using eq 7 ($6/V = 1.88 \times 10^{28}$ m^{-3}). At present, we explain the large concentration as follows. The hopping rate of the F1 ions at the boundary of a vacancy can be similar to that of the vacancy. Hence, both fast-moving vacancies and surrounding F1 ions can contribute to AC impedance and can thus be counted as carrier.

3.2. NMR Measurements. In this section, we examine the ^{19}F MAS NMR spectra of $Ce_{1-x}Sr_xF_{3-x}$. Figure 7 shows temperature dependence of ^{19}F MAS NMR spectra of pristine CeF_3 and $Ce_{1-x}Sr_xF_{3-x}$ (x = 0, 0.001, and 0.01). The isotropic signals of F1−F3 in pristine CeF_3 assigned on the basis of

https://doi.org/10.1021/acs.jpcc.2c06215
J. Phys. Chem. C 2022, 126, 20135−20142

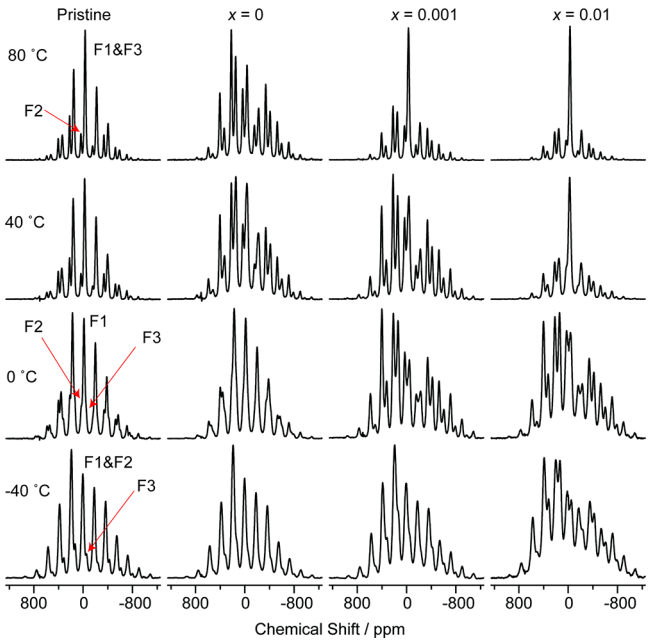

Figure 7. ^{19}F MAS NMR spectra at temperatures designated for each row. The first column is the spectra of pristine CeF_3 and the remaining three columns are those of $Ce_{1-x}Sr_xF_{3-x}$ with x = 0, 0.001, and 0.01, respectively.

spectral analysis described in ref 14 are indicated in the figure. Note that, for pristine CeF_3, the observed spectra below 100 °C can be modeled by the static MAS spectra calculated for F1−F3;[14] in other words, no motion is appreciable for F1−F3 in pristine CeF_3 below 100 °C. The apparent temperature-dependent lineshape for pristine CeF_3 is attributable to temperature-dependent thermally averaged magnetic moment of the unpaired electrons on Ce^{3+} (the Curie law).

Even below 100 °C, effects of F motion enhanced by Sr doping and milling−annealing become appreciable for $Ce_{1-x}Sr_xF_{3-x}$ (x = 0, 0.001, and 0.01) (Figure 7). For example, reduction of the F1 signal, which was observed at 240 °C for pristine CeF_3,[14] is appreciable for $Ce_{1-x}Sr_xF_{3-x}$ (x = 0.001) at 0 °C; it appears that the F1 signal is almost missing in the latter sample. With increasing temperature to 100 °C, a signal associated with a smaller number of sidebands emerges at the center of the spectrum. This peak is attributable to a signal from the F ions exchanging among F1−F3 sites.[14] Indeed, the relative intensity of F2 reduces concomitantly with the growth of the exchange peak. Similar but enhanced tendency is observed for $Ce_{1-x}Sr_xF_{3-x}$ (x = 0.01). These spectra thus show that F-ion motion is affected by Sr doping appreciably. In other words, the diffusion constant D_v in eq 5 depends on x, and the observed linear dependence of σ_{bulk} on x in Figure 4 is not solely governed by $C_v(x)$.

In the following, we estimate the exchange rate of F1 ions from the "F1 missing" spectrum of $Ce_{1-x}Sr_xF_{3-x}$ (x = 0.001) at 0 °C. For that, we briefly summarize effects of chemical exchange on a MAS sideband pattern in the following.[36,37] In the case of slow exchange ($2\pi\nu_R\tau_c \gg 1$, where ν_R is the MAS speed in Hz and τ_c is the correlation time of motion), the motion does not affect the formation of the rotational echo and a manifold of sharp sideband is observed. With increasing temperature, we encounter two intermediate exchange regimes. One is $2\pi\nu_R\tau_c \sim 1$, at which the formation of the rotational echo is disturbed by motion, leading to reduction of the signal. The other is $|2\pi\Delta\tau_c| \sim 1$, at which significant motional broadening and reduction of the signal due to short T_2 occurs. Here, Δ is the shielding anisotropy in Hz indicating spread of the signal by an anisotropic interaction. Finally, at fast exchange limit ($|2\pi\Delta\tau_c| \ll 1$), a narrow single signal appears at the isotropic chemical shift when the motion is isotropic. For anisotropic motion, we observe a new pattern reflecting a partially averaged anisotropic interaction. Indeed, such spectral change has been observed for CeF_3 by using a single crystal sample.[38] Note that for fast MAS case ($|\Delta/\nu_R| < 1$), we observe only the center band, which exhibits broadening at $2\pi\nu_R\tau_c \sim 1$.[39,40]

For F1 in pristine CeF_3 at 0 °C, we determined the principal values of the anisotropic interaction given as (δ_{XX}, δ_{YY}, δ_{ZZ}) = (452.0, 33.3, −542.3 ppm) and the isotropic shift δ_{iso} = −19 ppm.[14] Hence, the shielding anisotropy ($\Delta = \delta_{ZZ} - \delta_{iso}$) at 4.7 T is calculated to be ca. 100 kHz. Here, we assume that this Δ value can also be applicable to F1 in $Ce_{1-x}Sr_xF_{3-x}$ (x = 0.001). Since Δ is much larger than ν_R of 35 kHz ($|\Delta/\nu_R| \sim 3$), we encounter the two criteria of the intermediate region, $2\pi\nu_R\tau_c \sim 1$ and $2\pi\Delta\tau_c \sim 1$ successively with increasing temperature. The observed reduction of the F1 signal in the spectrum of $Ce_{1-x}Sr_xF_{3-x}$ (x = 0.001) at −40 °C is thus attributable to the case of $2\pi\nu_R\tau_c \sim 1$ and $|2\pi\Delta\tau_c| \sim 1$ is realized at around 0 °C, leading to the F1 missing spectrum. Let us examine the observed spectrum at 0 °C more quantitatively.

Figure 8a compares the observed spectrum (the black line) of pristine CeF_3 at 0 °C with the individual spinning sideband manifolds calculated for F1−F3 (F1: blue, F2: green, and F3: orange). Details of the lineshape calculation is given in ref 14. The intensity ratio of the individual spectra (F1:F2:F3 = 6:2:1) is consistent with the ratio of 12:4:2 per unit cell, showing that the observed spectrum is modeled by the calculation. In Figure 8b, we compare the observed spectrum (the black line) of $Ce_{1-x}Sr_xF_{3-x}$ (x = 0.001) at 0 °C with the calculated F1 and F3 spectra with the relative ratio of 2:1 (F2: green and F3: orange). These calculated spectra are the identical ones used in Figure 8a. The apparent fitting of the F2 and F3 spectra with the observed one in Figure 8b indicates that the F2 and F3 ions also remain stationary in $Ce_{1-x}Sr_xF_{3-x}$ (x = 0.001) at 0 °C. The remaining sharp signals in Figure 8b are different from the calculated pattern for F1 in Figure 8a and can be attributable to the F1 signal in the fast exchange limit ($|2\pi\Delta/\tau_c| \gg 1$), which we shall estimate in the following. We shall refer to the F1 ions in the fast exchange limit as $F1_{av}$.

To estimate the motionally averaged $F1_{av}$ signal, we assume that the exchange among crystallographically equivalent F1 sites reduces the size of the tensor (Δ) but its asymmetry ($\eta = (\delta_{YY} - \delta_{XX})/\Delta$) is retained. From ($\Delta$, η) = (522.6 ppm, 0.8) for F1 in CeF_3 at 0 °C, we estimated (Δ, η) = (466.7 ppm, 0.8) with δ_{iso} = −50.4 ppm for $F1_{av}$ in $Ce_{1-x}Sr_xF_{3-x}$ (x = 0.001) at 0 °C, and the calculated $F1_{av}$ spectrum is plotted in Figure 8c (the blue line) with the observed spectrum of $Ce_{1-x}Sr_xF_{3-x}$ (x = 0.001) at 0 °C (the black line). In the figure, we also plot the calculated sum spectrum (the red line), for which the three calculated signals of $F1_{av}$, F2, and F3 are mixed with the ratio of $F1_{av}$:F2:F3 = 0.4:2:1. Except for the discrepancy for the signals at around −200 ppm, which becomes apparent with the reduction of the F1 signal, the calculated spectrum explains the observed spectrum. The lower-frequency shift of δ_{iso} of $F1_{av}$ (δ_{iso} = −50.4 ppm) from δ_{iso} = −19 ppm for F1 in pristine CeF_3 is ascribable to averaging of the paramagnetic interaction by F1 motion. Indeed, a lower-frequency shift of the isotropic

https://doi.org/10.1021/acs.jpcc.2c06215
J. Phys. Chem. C 2022, 126, 20135−20142

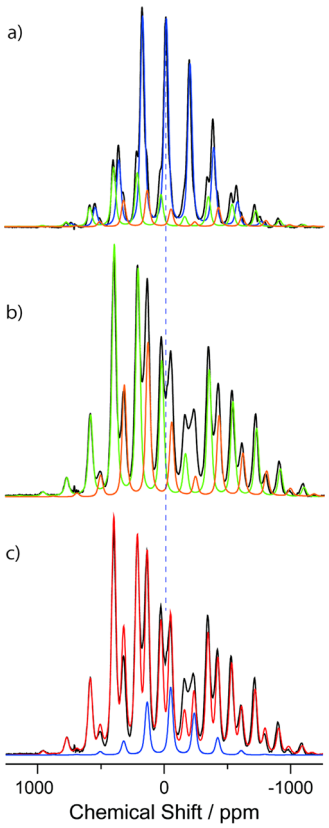

Figure 8. (a) Comparison between the observed ^{19}F MAS NMR spectrum (the black line) of pristine CeF_3 at 0 °C and the calculated spectra for F1 (blue), F2 (green), and F3 (orange) plotted with the relative intensity ratio of F1:F2:F3 = 6:2:1. Details of the lineshape calculation are given in Ref 14. (b) The observed spectrum of $Ce_{1-x}Sr_xF_{3-x}$ (x = 0.001) at 0 °C (the black line) is plotted with the calculated spectra of F2 (green) and F3 (orange), which are the same one plotted in (a), with the relative intensity ratio of F2:F3 = 2:1. (c) Comparison between the observed spectrum $Ce_{1-x}Sr_xF_{3-x}$ (x = 0.001) at 0 °C (the black line) with the calculated sum spectrum (the red line). The calculated F1 spectrum in the fast exchange limit is also plotted (the blue line). The vertical dotted line designates the position of the isotropic signal of F1 in pristine CeF_3 at 0 °C at −19 ppm.

chemical shifts of F1 in pristine CeF_3 with increasing temperature has been attributed to the reduction of the paramagnetic interaction (the Curie law).[14]

Figure 8c suggests that more than 90% of the F1 ions are in the intermediate region of $|2\pi\Delta\tau_c| \sim 1$, and their ^{19}F NMR signals are lost due to T_2 decay during the spin-echo time (~57 μs for ν_R = 35 kHz). We thus roughly estimate the F1−F1 exchange rate $k_F = 1/\tau_c$ among F1 in $Ce_{1-x}Sr_xF_{3-x}$ (x = 0.001) at 0 °C to be $k_F \sim 6 \times 10^5$ s^{-1} and use it to evaluate ionic conductivity σ in the following.

For evaluation of the diffusion constant of F1, we noted that Lee used the following expression for CeF_3[38]

$$D_F = \frac{1}{12}\frac{a^2}{\tau_c}, \tag{9}$$

which was originally introduced for LaF_3.[16,30] Sher et al. adopted the factor 1/12 rather than 1/6 because the diffusion affecting the ^{19}F−^{19}F dipolar interaction in LaF_3 is relative to other fluoride ions that are also diffusing. For CeF_3, since the ^{19}F lineshape is governed mostly by the electron−^{19}F dipolar interaction, we adopt the conventional definition of

$$D_F = \frac{1}{6}\frac{a^2}{\tau_c} \tag{10}$$

It is noted, however, that the factor 2 difference is not crucial in the following rough estimation of σ.

By putting a = 0.26 nm and $k_F = 6 \times 10^5$ s^{-1} in eq 10, we have $D_F = 6.76 \times 10^{-15}$ m^2/s. This value is one order higher than that estimated for pristine CeF_3 (~7×10^{-16} m^2/s) evaluated by using the activation parameters obtained by ^{19}F NMR.[38] The higher D_F value for $Ce_{1-x}Sr_xF_{3-x}$ (x = 0.001) is consistent with its higher conductivity. For the carrier density C_F, by assuming that all F1 ions are participating in the exchange, we have $C_F = 12/V \sim 3.74 \times 10^{28}$ m^{-3}. The conductivity with considering F1 as the carrier can be evaluated by rewriting eq 5 for F1 as

$$\sigma = \frac{e_0^2\, C_F\, D_F}{k_B\, T}. \tag{11}$$

The conductivity thus estimated becomes $\sigma = 1.7 \times 10^{-5}$ S/cm, which is consistent with the observed $\sigma_{bulk} = 1.43 \times 10^{-5}$ S/cm. Considering the coarse approximations we have employed, we admit that the good agreement is just coincidence, but the apparent consistency is enough to claim the legitimacy of applying eq 11 with F1 being the carrier for ion conduction in $Ce_{1-x}Sr_xF_{3-x}$ (x = 0.001) at 0 °C. Hence, the identity of the carrier viewed from the NMR lineshape experiment is clear; the carrier is the ^{19}F ions.

3.3. Effects of Different Timescale of Observation in the Two Measurements. It is notable that the hopping rate k_1 obtained by the AC impedance method is ca. 60 times faster than the F1−F1 exchange rate k_F estimated from the ^{19}F lineshape analysis. This can be explained in the framework of the so-called encounter model[41−44] for the NMR measurement as follows. F1−F1 exchange occurs when a vacancy migrating randomly among the F1 sites comes next the F1 ion (an encounter). The correlation time τ_c of the F1−F1 exchange is thus given by the mean time between two encounters. To advance consideration, we roughly estimate the characteristic timescale of ^{19}F lineshape observation as $T_c \sim 1/\Delta \sim 20$ μs, which allows more than 500 hopping for the vacancy with $k_1 = 3.5 \times 10^7$ s^{-1}. In fact, this estimation of T_c may be an underestimated one as the homogeneous line width of each spinning sideband (ca. 5 kHz for $Ce_{1-x}Sr_xF_{3-x}$ (x = 0.001) at 0 °C) leads $T_c \sim 100$ μs. Hence, the correlation time τ_c of the F1−F1 exchange is given by long-time average or ensemble average as

$$\tau_c = \tau C_F/C_v \tag{12}$$

where τ denotes the correlation time for the vacancy. Equation 12 leads

$$C_v D_v = C_F D_F \tag{13}$$

which allows us to use one of eqs 5 and 11, depending on the object of observation.

Here, we briefly comment on corrections of a correlation time obtained by NMR relaxation (T_1, T_2, and $T_{1\rho}$) experiments examined extensively in refs 41−44. Such corrections become necessary because the relaxation experiments observe a spin pair coupled by the dipolar interaction. Furthermore, T_1 and T_2 are sensitive to motional frequency

https://doi.org/10.1021/acs.jpcc.2c06215
J. Phys. Chem. C 2022, 126, 20135−20142

close to the Larmour frequency; the long-time average may not be applied. Spin diffusion during T_1 recovery or homonuclear Hartman−Hahn transfer during spin locking for $T_{1\rho}$ measurement should also be considered. Fortunately, these complexities can be avoided in the present lineshape analysis, and the simplified view presented above is applicable.

To conclude, the whole F1 ions contribute ion conduction as carrier at low temperature, and the enhanced conductivity by Sr doping is realized by the enhancement of F1 exchange motion by the introduction of vacancy. While the interpretation of "carrier" for the Nernst−Einstein relation (eqs 2 and 3) is clear in the lineshape analysis of ^{19}F NMR, the identity of carrier in the AC impedance method is rather elusive.

Lastly, we do not claim that the identification of the characteristic frequency in eq 1 being the carrier hopping rate is evidenced in this work. However, it is clear that the characteristic frequency certainly represents mobility of carriers and is useful for comparison of dynamics in conductivity among a series of materials. One example is the discussion about the best-fit slope of $(1.4 \pm 0.4) \times 10^{29}$ m^{-3}, which holds as long as the characteristic frequency is linearly proportional to the hopping rate.

4. CONCLUSIONS

Ion conduction in solids has been an important subject due, for example, to its application in all-solid-state batteries. To examine ion dynamics, both solid-state NMR and AC impedance measurements have been widely applied; however, comparison of their results is not straightforward. In this work, we examined ^{19}F NMR and AC impedance of CeF_3 and show that care must be taken to compare the results from the two measurements with apparently different timescales of observation and measurement objects.

In contrast to the case of LaF_3, for which MAS averages out the anisotropic interactions [^{19}F−^{19}F dipolar and ^{19}F chemical shielding anisotropies (CSA)] leaving three simple signals for F1−F3, the ^{19}F MAS spectrum of CeF_3 is consisted of spinning sideband patterns for F1−F3 characterized mostly by the large paramagnetic dipolar interaction among the unpaired electrons on Ce^{3+} and ^{19}F spins. Hence, for CeF_3, it is possible to deduce information of F1−F3 motion separately via analysis of the individual spinning sideband patterns. In this work, we estimated the F1−F1 exchange rate in Sr-doped $Ce_{1-x}Sr_xF_{3-x}$ (x = 0.001) at 0 °C as ca. 6×10^5 s^{-1}. By assuming F1−F1 exchange occurring between nearest neighbors, we evaluated the ionic diffusion constant D_F to be 6.76×10^{-15} m^2/s. Then, we applied the Nernst−Einstein relation to evaluate ion conductivity and showed that the observed conductivity can be realized by assuming all F1 ions in a unit cell act as "carrier". We further employed the AC impedance method to $Ce_{1-x}Sr_xF_{3-x}$ (x = 0.001) at 0 °C and obtained the carrier hopping rate of 3.5×10^7 s^{-1}, which is much faster than the F1−F1 exchange rate determined by NMR. The difference was explained in the framework of the so-called encounter model; the slower F1−F1 hopping rate observed in NMR is the result of the long-time average of the faster carrier hopping due to the long timescale of NMR lineshape observation. From the AC impedance method, the concentration of the carrier to realize the observed conductivity is much larger than that of the vacancy estimated from the ratio of Sr doping. For explanation, we postulate that not only ion vacancy but also fast-moving fluoride ions at the boundary of a vacancy do influence AC impedance.

AUTHOR INFORMATION

Corresponding Author

Miwa Murakami − *Office of Society-Academia Collaboration for Innovation, Kyoto University, Uji, Kyoto 611-0011, Japan*; orcid.org/0000-0001-6209-4450; Phone: +81-774-38-4967; Email: mmurakami@saci.kyoto-u.ac.jp; Fax: +81-774-38-4996

Authors

Seiya Matsumoto − *Department of Applied Chemistry, Graduate School of Engineering, University of Hyogo, Himeji, Hyogo 671-2201, Japan*

Atsushi Mineshige − *Department of Applied Chemistry, Graduate School of Engineering, University of Hyogo, Himeji, Hyogo 671-2201, Japan*

Complete contact information is available at: https://pubs.acs.org/10.1021/acs.jpcc.2c06215

Notes

The authors declare no competing financial interest.

ACKNOWLEDGMENTS

This article is based on results of the projects RISING2 (JPNP16001) and RISING3 (JPNP21006), commissioned by the New Energy and Industrial Technology Development Organization (NEDO). The authors thank Prof. K. Takegoshi at Kyoto University for the use of the 4.7 T NMR magnet. The F1 network structure in Figure 3 was prepared using VESTA.[45]

REFERENCES

(1) Afanasiev, M. L.; Habuda, S. P.; Lundin, A. G. The symmetry and basic structures of LaF_3, CeF_3, PrF_3 and NdF_3. *Acta Crystallogr., Sect. B: Struct. Sci., Cryst. Eng. Mater.* **1972**, *28*, 2903−2905.

(2) Cheetham, A. K.; Fender, B. E. F.; Fuess, H.; Wright, A. F. A powder neutron diffraction study of lanthanum and cerium trifluorides. *Acta Crystallogr., Sect. C: Cryst. Struct. Commun.* **1976**, *32*, 94−97.

(3) Gregson, D.; Catlow, C. R. A.; Chadwick, A. V.; Lander, G. H.; Cormack, A. N.; Fender, B. E. F. The structure of LaF_3 - a single-crystal neutron diffraction study at room temperature. *Acta Crystallogr., Sect. B: Struct. Sci., Cryst. Eng. Mater.* **1983**, *39*, 687−691.

(4) Maximov, B.; Schulz, H. Space group, crystal structure and twinning of lanthanum trifluoride. *Acta Crystallogr., Sect. B: Struct. Sci., Cryst. Eng. Mater.* **1985**, *41*, 88−91.

(5) Zalkin, A.; Templeton, D. H. Refinement of the trigonal crystal structure of lanthanum trifluoride with neutron diffraction data. *Acta Crystallogr., Sect. B: Struct. Sci., Cryst. Eng. Mater.* **1985**, *41*, 91−93.

(6) Nagel, L.E.; O'Keeffe, M.Fast Ion Transport in Solids, in: W., van Gool (Eds.), *Solid State Batteries and Devices*; North Holland Publishing Co., Amsterdam, 1973, pp. 165−172.

(7) Takahashi, T.; Iwahara, H.; Ishikawa, T. Ionic Conductivity of Doped Cerium Trifluoride. *J. Electrochem. Soc.* **1977**, *124*, 280−284.

(8) Omari, M. E.; Sénégas, J.; Réau, J.-M. Ionic conductivity properties and ^{19}F NMR investigation of $Ln_{1-y}Cd_yF_{3-y}$ (Ln = Ce, Nd) solid solutions with tysonite-type structure. Part I: Ionic conductivity properties. *Solid State Ionics* **1998**, *107*, 281−291.

(9) Sorokin, N. I.; Sobolev, B. P. Nonstoichiometric Fluorides—Solid Electrolytes for Electrochemical Devices: A Review. *Crystallogr. Rep.* **2007**, *52*, 842−863.

(10) Sorokin, N. I.; Sobolev, B. P. Frequency Response of the Low-Temperature Ionic Conductivity of Single Crystals $R_{1-y}M_yF_{3-y}$ (R = La−Er; M= Ca, Sr, Ba, Cd). *Phys. Solid State* **2008**, *50*, 416−421.

(11) Sorokin, N. I.; Smirnov, A. N.; Fedorov, P. P.; Sobolev, B. P. Supersonic Fluoride Ceramics RF_3 and $R_{0.95}Sr_{0.05}F_{2.95}$ (R = La, Ce, Pr, Nd) Prepared by Hot Pressing. *Russ. J. Electrochem.* **2009**, *45*, 606−608.

(12) Dieudonné, B.; Chable, J.; Body, M.; Legein, C.; Durand, E.; Mauvy, F.; Fourcade, S.; Leblanc, M.; Maisonneuve, V.; Demourgues, A. The key role of the composition and structural features in fluoride ion conductivity in tysonite $Ce_{1-x}Sr_xF_{3-x}$ solid solutions. *Dalton Trans.* **2017**, *46*, 3761−3769.
(13) Wang, F.; Grey, C. P. Probing the Mechanism of Fluoride-Ion Conduction in LaF_3 and Strontium-Doped LaF_3 with High-Resolution ^{19}F MAS NMR. *Chem. Mater.* **1997**, *9*, 1068−1070.
(14) Murakami, M.; Mineshige, A. ^{19}F NMR studies on ionic conduction pathways in tysonite-CeF_3. *J. Phys. Chem. Solids* **2022**, *161*, No. 110432.
(15) Schoonman, J.; Oversluizen, G.; Wapenaar, K. E. D. Solid electrolyte properties of LaF_3. *Solid State Ionics* **1980**, *1*, 211−221.
(16) Lee, K.; Sher, A. F^{19} Nuclear Magnetic Resonance Line Narrowing in LaF_3 at 300 °K. *Phys. Rev. Lett.* **1965**, *14*, 1027−1029.
(17) Roos, A.; Aalders, A. F.; Schoonman, J.; Arts, A. F. M.; de Wijn, H. W. Electrical conduction and ^{19}F NMR of solid solutions $La_{1-x}Ba_xF_{3-x}$. *Solid State Ionics* **1983**, *9-10*, 571−574.
(18) Roos, A.; van de Pol, F. C. M.; Keim, R.; Schoonman, J. Ionic Conductivity I tysonite-type solid solutions $La_{1-x}Ba_xF_{3-x}$. *Solid State Ionics* **1984**, *13*, 191−203.
(19) Breuer, S.; Gombotza, M.; Pregartnera, V.; Hanzua, I.; Wilkeninga, M. Heterogeneous F anion transport, local dynamics and electrochemical stability of nanocrystalline $La_{1-x}Ba_xF_{3-x}$. *Energy Storage Mater.* **2019**, *16*, 481−490.
(20) Almond, D. P.; Dunkan, G.; West, A. R. The determination of hopping rates and carrier concentrations in ionic conductors by a new analysis of ac conductivity. *Solid State Ionics* **1983**, *8*, 159−164.
(21) Almond, D. P.; West, A. R. Impedance and modulus spectroscopy of "real" dispersive conductors. *Solid State Ionics* **1983**, *11*, 57−64.
(22) Almond, D. P.; West, A. R. Mobile ion concentrations in solid electrolytes from an analysis of a.c. conductivity. *Solid State Ionics* **1983**, *9-10*, 277−282.
(23) Privalov, A. F.; Vieth, H.-M.; Murin, I. V. Nuclear magnetic resonance study of superionic conductors with tysonite structure. *J. Phys.: Condens. Matter* **1994**, *6*, 8237−8243.
(24) Chable, J.; Dieudonné, B.; Body, M.; Legein, C.; Crosnier-Lopez, M.-P.; Galven, C.; Mauvy, F.; Durand, E.; Fourcade, S.; Sheptyakov, D.; et al. Fluoride solid electrolytes: investigation of the tysonite-type solid solutions $La_{1-x}Ba_xF_{3-x}$ ($x < 0.15$). *Dalton Trans.* **2015**, *44*, 19625−19635.
(25) Breuer, S.; Lunghammer, S.; Kiesl, A.; Wilkening, M. F anion dynamics in cation-mixed nanocrystalline LaF_3: SrF_2. *J. Mater. Sci.* **2018**, *53*, 13669−13681.
(26) MacDonald, J. R. New aspects of some small-signal ac frequency response functions. *Solid State Ionics* **1985**, *15*, 159−161.
(27) Takeda, K. OPENCORE NMR: Open-source core modules for implementing an integrated FPGA-based NMR Spectrometer. *J. Magn. Reson.* **2008**, *192*, 218−229.
(28) Brey, W.S.; Brey, M.L.Fluorine-19 NMR. In *Encyclopedia of Nuclear Magnetic Resonance*; 2011; Vol.3; pp. 2063−2071; Grant, D.M.; Harris, R.K., eds.; John Wiley and Sons.
(29) Bielecki, A.; Brum, D. P. Temperature Dependence of ^{207}Pb MAS Spectra of Solid Lead Nitrate. An Accurate, Sensitive Thermometer for Variable-temperature MAS. *J. Magn. Reson., Ser. A* **1995**, *116*, 215−220.
(30) Sher, A.; Solomon, R.; Lee, K.; Muller, M. W. Transport Properties of LaF_3. *Phys. Rev.* **1966**, *144*, 593−604.
(31) Aalders, A. F.; Arts, A. F. M.; de Wijn, H. W. Vacancy distribution and ionic motion in LaF_3 studied by ^{19}F NMR. *Phys. Rev.* **1985**, *32*, 5412−5423.
(32) Omari, M. E.; Sénégas, J.; Réau, J.-M. Ionic conductivity properties and 19F NMR investigation of Ln1-yCdyF3-y (Ln = Ce, Nd) solid solutions with tysonite-type structure. Part II: 19F NMR investigation. *Solid State Ionics* **1998**, *107*, 293−305.
(33) Privalov, A. F.; Vieth, H.-M.; Murin, I. V. Ionic motion in the LaF_3 superionic conductor studied by ^{19}F NMR with homonuclear decoupling. *J. Phys. Chem. Solids* **1989**, *50*, 395−398.
(34) Goldman, M.; Shen, L. Spin-spin relaxation in LaF_3. *Phys. Rev.* **1966**, *144*, 321−331.
(35) Brach, I.; Schulz, H. Determination of the diffusion path in the ionic conductor LaF_3. *Solid State Ionics* **1985**, *15*, 135−138.
(36) Schmidt, A.; Smith, S. O.; Raleigh, D. P.; Roberts, J. E.; Griffin, R. G.; Vega, S. Chemical exchange effects in the NMR spectra of rotating solids. *J. Chem. Phys.* **1986**, *85*, 4248−4253.
(37) Schmidt, A.; Vega, S. NMR line shape analysis for two-site exchange in rotating solids. *J. Chem. Phys.* **1987**, *87*, 6895−6907.
(38) Lee, K. Fluorine-19 nuclear magnetic resonance in CeF_3. *Solid State Commun.* **1969**, *7*, 367−371.
(39) Maricq, M. M.; Waugh, J. S. NMR in rotating solids. *J. Chem. Soc.* **1979**, *70*, 3300−3316.
(40) Suwelack, D.; Rothwell, W. P.; Waugh, J. S. Slow molecular motion detected in the NMR spectra of rotating solids. *J. Chem. Phys.* **1980**, *73*, 2559−2569.
(41) Eisenstadt, M.; Redfield, A. G. Nuclear Spin Relaxation by Translational Diffusion in Solids. *Phys. Rev.* **1963**, *132*, 635−643.
(42) Wolf, D. Determination of self-diffusion mechanisms from high-field nuclear-spin-relaxation experiments. *Phys. Rev.* **1974**, *10*, 2710−2723.
(43) Wolf, D. Effect of correlated self-diffusion on the low-field nuclear-spin relaxation in the rotating reference frame. *Phys. Rev.* **1974**, *10*, 2724−2732.
(44) Messer, R.; Birli, H.; Schimmele, L. Haven ratio and correlation effects in diffusion in Li_3N. *Radiat. Eff.* **1983**, *75*, 151−157.
(45) Momma, K.; Izumi, F. *VESTA 3* for Three-Dimensional Visualization of Crystal, Volumetric and Morphology Data. *J. Appl. Crystallogr.* **2011**, *44*, 1272−1276.

https://doi.org/10.1021/acs.jpcc.2c06215
J. Phys. Chem. C 2022, 126, 20135−20142